

FATIGUE-CREEP-ENVIRONMENT INTERACTIONS IN A DIRECTIONALLY-SOLIDIFIED NI-BASE SUPERALLOY

A.P. Gordon¹, R.W. Neu^{1,2}, and D.L. McDowell^{1,2}

¹George W. Woodruff School of Mechanical Engineering, Georgia Tech, Atlanta GA 30332-0405

²School of Materials Science and Engineering, Georgia Tech, Atlanta GA 30332-0245

ABSTRACT

Directionally-solidified (DS) GTD-111 is a Ni-base superalloy designed to withstand damage occurring in the first and second stage blades of gas-powered turbines. Because of the distinctive microstructure of this material, the manner in which fatigue-creep-environment damage mechanisms interact to initiate cracks is sensitive to grain structure and chemical composition. Along with fatigue cycling, certain high temperature components such as blades are subjected to sustained dwell periods (i.e., creep) either in tension or compression. Experiments have been carried out to simulate a variety of thermal, mechanical, and environmental operating conditions endured by longitudinally (L) and transversely (T) oriented DS GTD-111. Tests in extreme environments/temperatures were needed to isolate one or at most two of the damage mechanisms. Microscopy along with strain-life data were then used to map the damage mechanisms occurring in both orientations of the as-cast, and in several cases pre-exposed material, subjected to creep-fatigue conditions.

Introduction

Nickel-base superalloys are technologically significant materials that are used extensively in applications that require high strength, along with resistance to creep, fatigue, and corrosion even at elevated temperatures. Specialized processing techniques are employed to enhance mechanical properties; hence, a prime example is the elimination of grain boundaries along the turbine blade axis via directional solidification. This method, however, introduces new challenges in characterizing the damage and crack initiation life behaviors. Directionally-solidified GTD-111 is a relatively recently-developed Ni-base superalloy for turbine applications. The initial microstructure of a bucket is the product of composition, casting, and heat treatment. The service conditions in these components, which generally exceed 600°C, facilitate the onset of one or more damage mechanisms. A variety of creep-fatigue testing configurations, which simulate service conditions, is used to either draw out or isolate the damage mechanisms common to Ni-base superalloys. Since damage varies with cycle type, orientation, temperature, prior exposure, atmosphere, etc., observations from micrographs of sections of tested samples have been used to develop damage mechanism maps (DMMs). The DMMs quantify the transitions between damage mechanism regimes and can be applied to develop physically-based crack initiation models.

Damage Mechanisms of Ni-base Superalloys

Grains of DS GTD-111 can measure above 100mm in length along the DS axis and are approximately 5mm in width transverse to the DS axis. Like other Ni-base superalloys, DS GTD-111 is a dual-phase intermetallic consisting of a soft matrix and hard precipitates. The γ matrix phase is FCC austenitic Ni solid solution with strengthening elements. The L1₂-structured γ' precipitate phase is an ordered FCC super-lattice of nickel-aluminide, Ni₃Al, having a bimodal distribution. Cuboidal γ' precipitate particles average 0.5 μ m in width. During the solidification process, primary dendrite stems grow parallel to the solidification direction. These stems are accompanied by secondary and tertiary dendrite arms that grow outward along [100] and [010] directions. Nickel-base superalloys with the DS structure derive anisotropic and superior creep resistance the solidification process. Void nucleation and sliding at the GBs that are common to polycrystalline materials are each limited in DS Ni-base superalloys since the presence of GBs perpendicular to the primary stress direction (L-oriented) is eliminated [1]. Directionally-solidified GTD-111 contains MC-type carbides that are present just after casting, and it also contains M₂₃C₆-type carbides which develop during ageing. Each type of inclusion particle is most prevalent between adjacent dendrites (e.g. in the so-called interdendritic region), in the γ matrix, along GBs, and near air-exposed surfaces.

Numerous damage mechanisms lead to the generation and early propagation of cracks in materials subjected to high temperature fatigue. A variety of stress concentrators (e.g. casting pores, inclusions, and grain boundaries) typically exist within the bulk of cast Ni-base superalloys. Fatigue cycling leads to enhanced slip band formation and cracking at these sites.

Microcracks can originate from micropores formed due to the nature of the solidification processes. Carbide inclusions or other large "nodules", especially those which are plentiful at grain boundaries, can fracture or debond. Under creep conditions, crack coalescence leads to transgranular crack growth and failure of Ni-base superalloys [2-4]. When this mechanism operates the size distribution of rogue inclusions, pores, and surface features are important parameters.

Surfaces of materials exposed to corrosive surroundings are prone to absorbing reactive elements from the environment. Such is the case with Ni-base superalloys in which exposed regions sustain compositional changes that alter the local properties. Oxidation intrusion of bare Ni-base samples generally consists of two stages [5]: rapid growth during the initial transition period and slow stable growth during the subsequent period. Chemicals diffuse from grain boundaries, interdendritic regions, and γ' particles in close proximity to the external surface. The formation of several adjacent oxide scales in the form of TiO_2 , Cr_2O_3 , Al_2O_3 , etc. depends on the initial concentration of Ti, Cr, Al, etc., respectively. The accumulated oxidation clogs diffusion pathways, thereby slowing oxide formation to a steady-state. With continued exposure time, the external scales are discernable via various forms of microscopy. A continuous chromia layer typically forms on the outer surface and is separated from the metal by non-uniform alumina particles. As the result of Al and Ti being stripped from γ' particles, a ductile matrix layer referred to as the γ' -depleted zone, is formed underneath the cumulative oxide scale.

Oxide layers display brittle characteristics in the operating temperatures of hot path turbine blades; therefore, in the presence of mechanical loading, or even thermal loading, surface oxides may fracture suddenly. Under tensile deformation, the mismatch in elastic modulus at the oxide/metal interface results in localized stresses which often exceed the critical fracture strength of the oxide [6-8]. Scale fracture exposes the local subjacent virgin metal which itself oxidizes and cracks. The cumulative effects of oxidation-assisted surface crack initiation are oxide spikes that protrude into the bulk material. Under isothermal fatigue conditions, oxide spiking lowers the overall ductility of the material [9-11]. Microcracks nucleate early along surface due to the lower fracture toughness of this surface layer. Eventually a few of these oxide-spikes penetrate into the bulk material, possibly due to interdendritic oxidation (relating to the heterogeneity of the local oxidation kinetics), one or more of which form the catastrophic crack.

Continuous cycling experiments under various isothermal conditions were conducted in a previous study [12]. In the present investigation, creep-fatigue experiments are performed under strain-controlled loading to investigate the time-sensitive behavior of the damage mechanisms on the overall crack initiation behavior of DS Ni-base superalloys. It is expected that by modifying the test conditions (i.e., dwell time, dwell type, and environment) the contribution of the damage mechanism leading to crack initiation will be influenced. The effects of pre-exposing the material will also alter the balance of the contributions of the damage mechanisms.

Experimental Methodology

Isothermal low cycle fatigue (LCF) tests with super-imposed dwell periods were conducted on DS GTD-111. The experimental procedure for these so-called creep-fatigue tests is identical to continuous cycling LCF testing except for the addition of either tensile or compressive holds. For tests with tensile dwell periods, the specimen is held at the peak tensile strain for a time period, t_{ht} . Similarly, for tests with compressive holds, the specimen is held at the peak compressive strain for a time period, t_{hc} . Various temperatures and strain range combinations were used to conduct tests on L- and T-oriented DS GTD-111 specimens. Hold periods of 2 or 10 min were used. To measure cycles to crack initiation life, N_i , each test was carried out until a 20% load drop occurred. With a strain rate of 0.5%/s for each test, a 2 min hold period accounts for at least 85% of the total cycling time even for large strain ranges. Data from creep rupture and deformation tests that were conducted on DS GTD-111 in an earlier study are also relevant to the current investigation (Ibanez, 2003).

The experimental setup used for isothermal LCF and creep-fatigue testing was modified to conduct several experiments in a semi-inert gaseous environment. A semi-closed chamber was fabricated to house the specimen, induction coils, and extensometer tips. Using a gas regulator, Argon was supplied to the chamber at a pressure of nearly 34 kPa (5 psi) so that gas would always be flowing out of the chamber. The real-time oxygen content of the chamber was measured with a laser-based oxygen sensor. In this manner the oxygen content of the chamber was maintained at 2% during fatigue testing.

To investigate the effect of pre-exposure on crack initiation life, several LCF specimens were pre-exposed in air at high temperature, and in some cases a static load was applied. To simulate the corrosive effects of the syngas environment, several specimens were subjected to a sulfur-rich pre-exposure. Pre-exposure consisted of a specified temperature (982°C for all cases), mechanical load (0, or $\pm 100\text{MPa}$), and environment (air or simulated syngas) for 100 hr. Pre-exposure in the simulated syngas environment was conducted using N_2 with 100 ppm H_2S . In the stressed cases that were carried out on the servo-hydraulic machine, creep deformation occurred and was recorded. The specimens were subsequently tested under LCF conditions to determine the effect of pre-exposure on fatigue crack in initiation life.

Results

Under creep-fatigue conditions in air, crack initiation lives of both L- and T-oriented DS GTD-111 are less than those that were obtained under continuous cycling but otherwise identical conditions as shown in Fig. 1. For a given set of experimental conditions (i.e., T , R_ε , $\Delta\varepsilon$, and $\dot{\varepsilon}$) the plastic strain ranges of hold in compression (HC) and hold in tension (HT) cases were larger than those from continuous cycling (CC) conditions, and the crack initiation lives were shorter. The interpolated $\Delta\varepsilon$ - N_i curves for either HC or HT cases exist entirely beneath CC strain-life curves for the L-oriented material. At the lower temperature (871°C), the lowest N_i values were obtained for compression creep-fatigued cases; however, for the higher temperatures, N_i was lowest for HT cases. Crack initiation lives under HT outlast those under HC by nearly a factor of 2 for either grain orientation at 871°C. Alternately, crack initiation lives under HC and CC outlast those under HT by nearly a factor of 5 for either grain orientation at 1038°C. This crossover of crack initiation life corresponds to a changeover in dominant damage mechanisms when cycling under CC, HC, and HT.

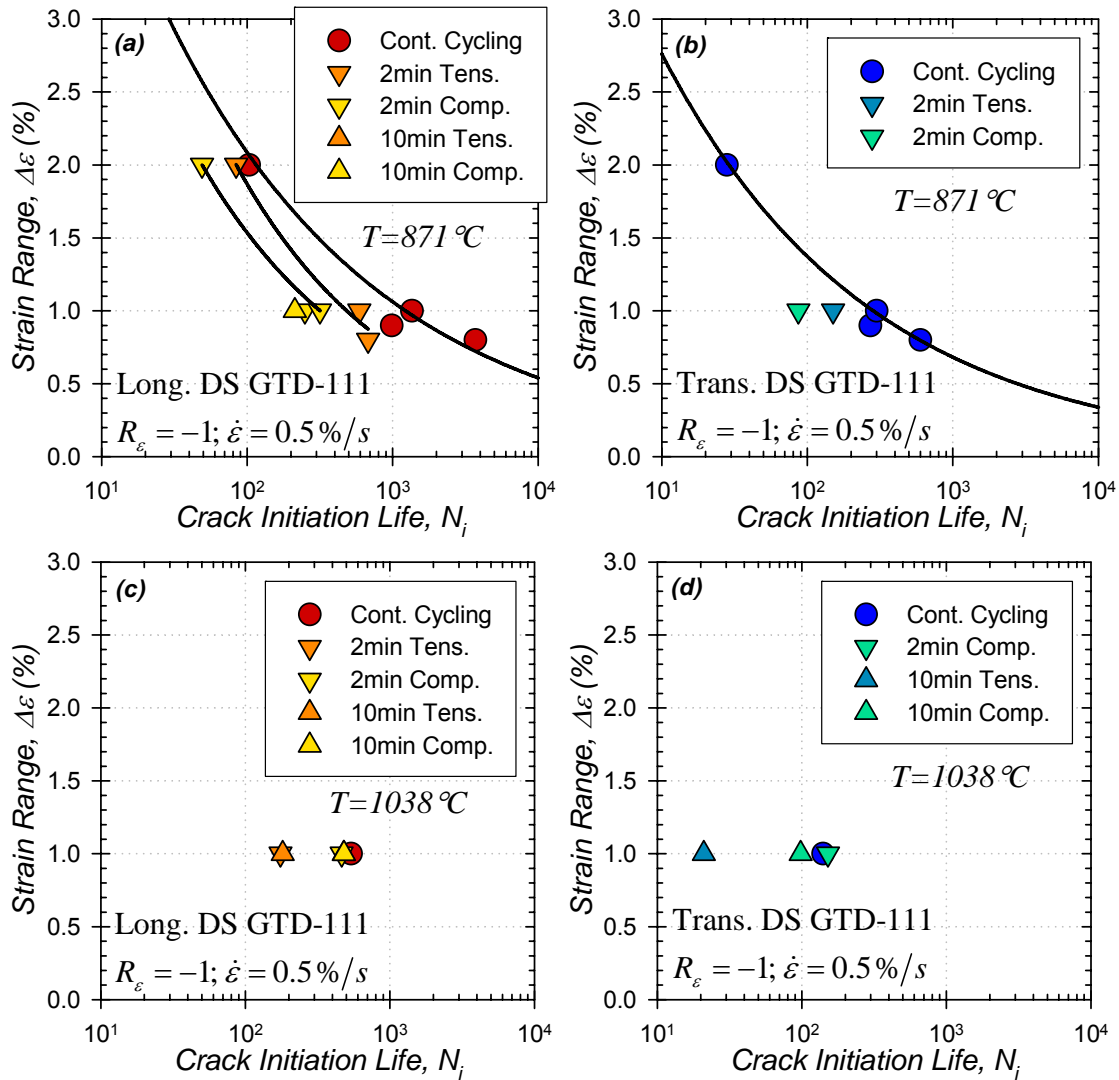


Figure 1: Crack initiation lives of (a, c) L-oriented and (b, d) T-oriented DS GTD-111 under continuous and creep-fatigue cycling.

Visual comparison of the profiles of fatigued samples can be used to determine which mechanism is responsible for promoting crack nucleation. As shown in Fig. 2 the material has limited surface cracking under CC. Under creep-fatigue conditions, specimens contain numerous surface cracks. Surface cracks in the HC-tested case occurred often and are aligned transverse to the stress axis, whereas cracks in the HT-tested material are wavy and are lesser in number. In this manner, microscopy was applied to characterize the damage mechanisms.

Crack initiation under creep-fatigue cycling with compressive dwells, as shown in Fig. 3a, was facilitated by the ingress of surface oxides. During cyclic reversals the typically brittle accumulated oxide layer fractures in tension and exposes subjacent virgin material. Once this newly-oxidized material fractures, the process repeats. The result is the formation of a series of oxide spikes propagating transverse to the direction of the applied load.

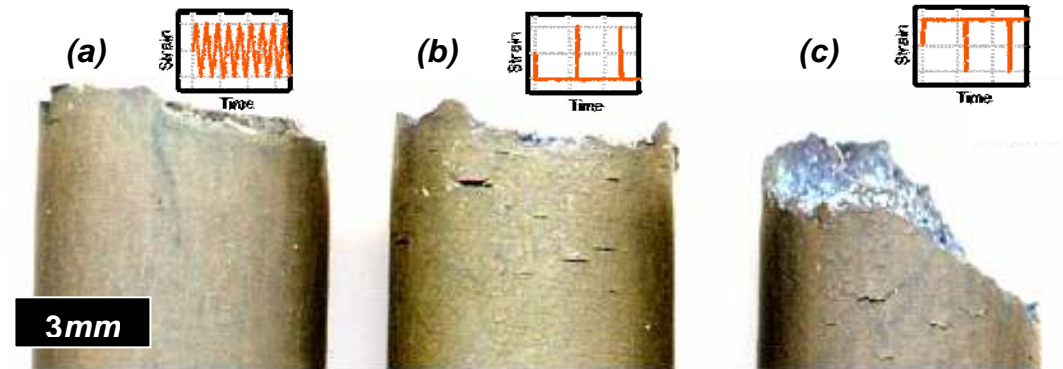


Figure 2: Effect of cycle type on fracture profile of L-oriented DS GTD-111 with $\Delta\varepsilon = 0.8\%$, $R_\varepsilon = -1$, $\dot{\varepsilon} = 0.5\%/s$, and 871°C .

The HT-tested sample displays a different mechanism dominating the crack nucleation process, as shown in Fig. 3b. Subsurface carbides in the interdendritic channels were the main cause of crack initiation. The main crack propagated by coalescing with adjacent microcracks. The randomized nature of the carbides networks and their morphologies lead to non-planar cracking. In nearly all cases the carbides themselves did not fracture. Their non-linear profile indicates that the initiation and early propagation phases are controlled by inclusions and other contaminants found in the interdendritic regions. Relative to the HC case, the HT-tested profiles more closely resembles CC cases even though the lives differ.

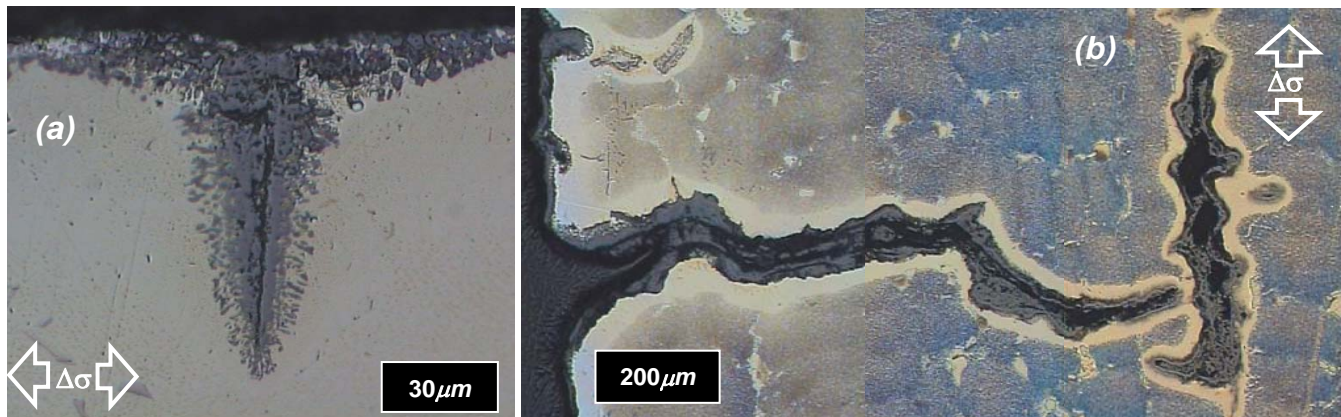


Figure 3: Crack initiation in DS GTD-111 caused by 10min dwell periods under (a) HC and (b) HT. For each case $\dot{\varepsilon} = 0.5\%/s$, $R_\varepsilon = -1$, $\Delta\varepsilon = 1.0\%$, and $T=1038^\circ\text{C}$.

Directionally-solidified GTD-111 samples under compression creep-fatigue cycling in a semi-inert environment exhibited longer lives than those tested in air by a factor of 1.4, as shown in Fig. 4. The Ar-tested strain-life curve approaches that of the CC case which serves as an upper bound on life since they are not influenced by environment. Based on this effect, it can be assumed that further decreasing the presence of oxygen in the environment (e.g. by means of vacuum testing) would further increase the crack initiation life of the material.

Decreasing the concentration of the diffusing species present in the environment (e.g. oxygen) limits the environmental-fatigue crack initiation mechanism and thus increases the crack initiation life of the test material. At 871°C , the semi-inert environment limited the formation of surface oxides that would lead to oxide spiking in air. Although the small amount of oxygen present in the Ar-rich environment lead to the formation of a very thin (e.g. $9\mu\text{m}$) oxide layer, the crack initiation mechanism was influenced by subsurface features, as shown in Fig. 5. Increasing the strain range from 0.8% to 1.0% both increases the plastic strain range and decreases the number of cracks present at the surface. The cracks at the higher strain range appear wavy and the oxide layer formed at the surface is thinner.

The effect of prior exposure on crack initiation life of L- and T-oriented DS GTD-111 was investigated using a standard pre-exposure time, $t_{pre}=100hr$, and temperature, $T_{pre}=982^{\circ}C$. While most specimens were pre-exposed in static air, two specimens were exposed to wet H_2S that simulated the gasified operating environment of DS GTD-111 turbine blades. Additionally, while most specimens were pre-exposed under no load, several were subjected to static pre-loads of either $\pm 100MPa$. Afterwards, each sample was continuously fatigue cycled at $871^{\circ}C$, with $R_{\epsilon}=-1$ and $\dot{\epsilon}=0.5\%/s$. The resultant effect of pre-exposure on the reduction of the crack initiation lives of DS GTD-111 is a direct consequence of the degraded material and its mechanical properties. The effect of pre-exposure on life is shown in Fig. 6. Of all of the cases subjected to no pre-load whatsoever, those previously exposed in air have the least detrimental effect on life. Increasing the aggressive nature of the pre-exposure environment from air to H_2S had the effect of increasing the oxide penetration which further decreased life. These reductions were exhibited by both the L- and T-oriented specimens. Pre-exposing the L-oriented material to either $0MPa$ or $-100MPa$ in air had approximately the identical effect, i.e., a factor of 2 reduction in life. Formation of subsurface cracks caused by tensile creep (e.g. $100MPa$), however, severely lowered the crack initiation life of the material.

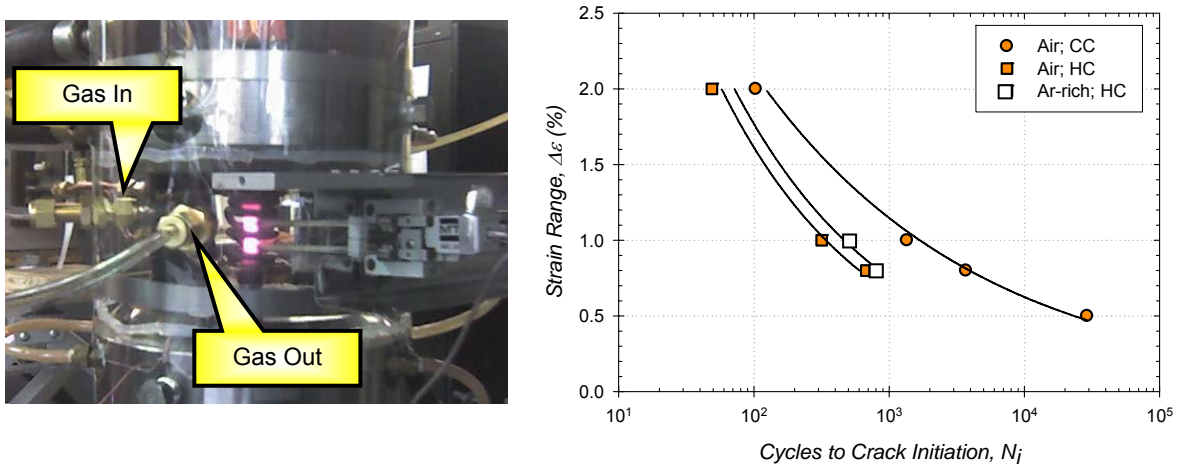


Figure 4: (a) Gas chamber used in alternate environment testing. (b) Effect of environment on crack initiation of L-oriented DS GTD-111 at $871^{\circ}C$, $R_{\epsilon}=-1$, and $\dot{\epsilon}=0.5\%/s$.

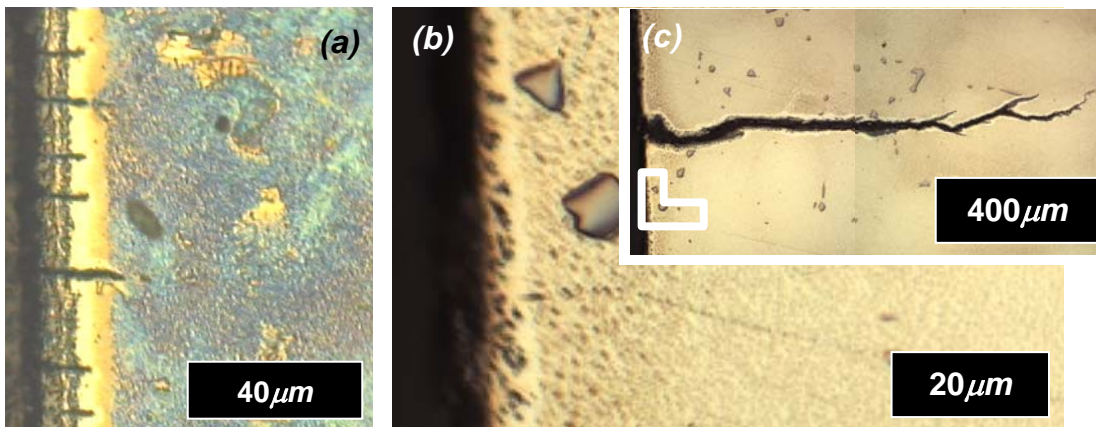


Figure 5: Effect of environment on damage mechanisms leading to crack initiation. For each case $T=871^{\circ}C$, HC (2min), $R_{\epsilon}=-1$, $\Delta\epsilon=0.8\%$, $\dot{\epsilon}=0.5\%/s$, (a) air (b, c) argon-rich environment.

The most noticeable effects of exposing Ni-base superalloys to high temperature conditions either with or without pre-loading can be categorized as those affecting the surface or those affecting the subsurface. When DS GTD-111 is exposed to $982^{\circ}C$ for 100 hours in static laboratory air, for example, an oxide layer measuring approximately $11\mu m$ forms on the surface. The presence of the oxide layer prior to fatigue cycling alters the diffusion and damage processes near the surface and influences the mechanics of crack initiation of the material.

The crack initiation behavior of the material is influenced by not only the cumulative oxide layer, but also the γ' -depleted zone, as shown in Fig. 7. Upon fatigue cycling, the oxide layer and the ductile γ' -depleted zone (i.e., essentially a matrix layer

containing fine Ni₃Al particles), forms wide cracks that arrest at the virgin material. The stress concentrations at these early-formed crack tips initiate the oxide spiking damage mechanism. Under these identical LCF conditions without prior exposure, the oxide spiking damage mechanism does not occur in DS GTD-111. Pre-exposing the material in the H₂S environment lead to deeper ingression of both layers compared to the air-exposed case. In both cases shown, surface-initiated cracking was the dominant cause of damage. Multiple hairline cracks emanated from early-formed matrix cracks and extend into the bulk of the material. Very little oxidation formed on the interior fracture surfaces in either case since the cracks advanced quickly and since the fatigue temperature was low. Since the surface degradation was more aggressive in the H₂S-exposed case, the accumulated initial cracks in the matrix layer are more plentiful and extend more deeply into the bulk of the material compared to the air-exposed case.

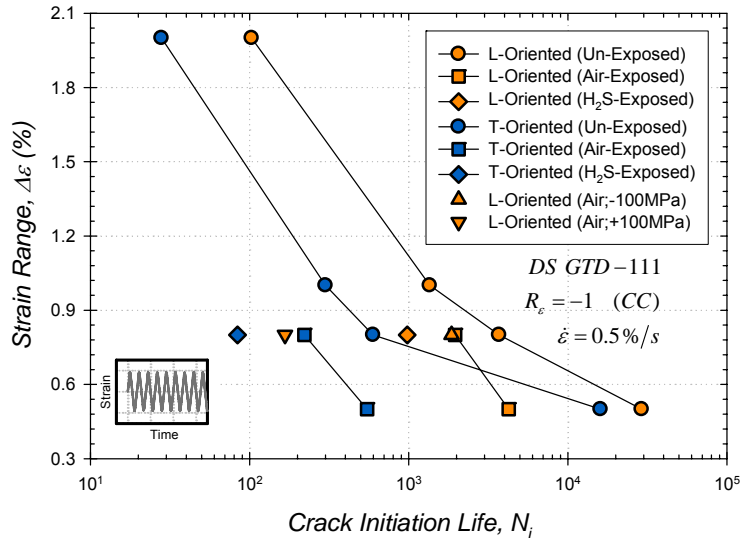


Figure 6: Pre-exposure effects on crack initiation behavior of L-oriented DS GTD-111 in static air under (a) pre-exposure only (100hr, 982°C, 100MPa), (b) pre-exposure (100hr, 982°C, 100MPa) and fatigue ($\Delta\epsilon=0.5\%$ and 871°C), and (c) pre-exposure (100hr, 982°C, -100MPa) and fatigue ($\Delta\epsilon=0.8\%$ and 871°C).

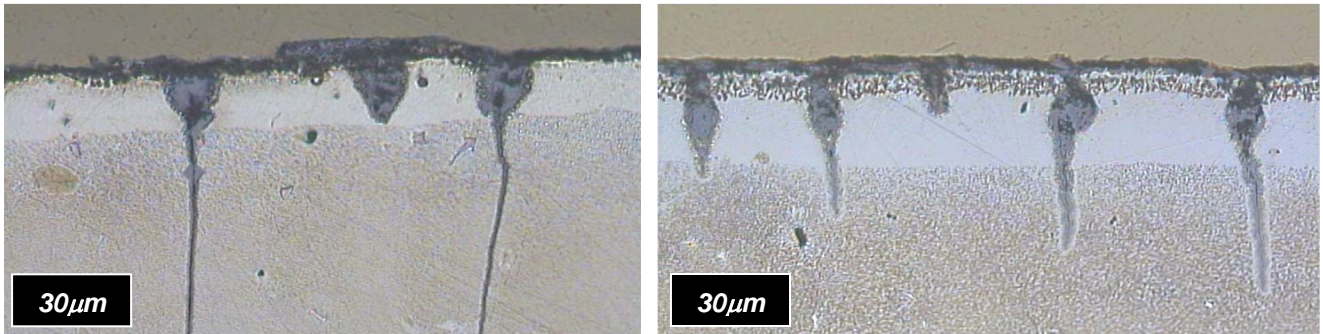


Figure 7: Microstructures of (a) air and (b) H₂S-exposed L-oriented DS GTD-111. Pre-exposure conditions: 982°C, 100hr, 0MPa. Fatigue cycling conditions: $\Delta\epsilon=0.8\%$, 871°C, and $\dot{\epsilon} = 0.5\%/s$.

Figure 8 compares the microstructures of the two pre-crept and fatigued samples. Common to the surface of each material is the accumulated oxidation layer. Oxides spalled from the majority of the surface area of the case pre-crept in compression. For the case pre-crept in tension, numerous microcracks were found beneath the surface. Upon fatigue cycling, cracks emanating from the surface coalesced with those initiated at the subsurface, thus creating a non-planar fracture path. These subsurface cracks do not form in the compressively pre-crept case; therefore, the crack initiation behaves much like the pre-heated/unloaded cases. In both of the pre-crept cases rafting occurred. These raft-shaped particles measure five times the original length of the cuboidal precipitate particles. Transmission electron microscopy (TEM) is needed to precisely determine the effect of rafting on the deformation behavior of the material.

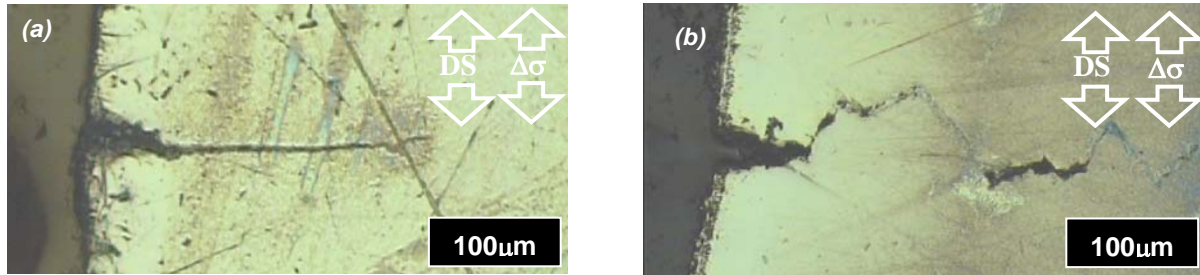


Figure 8: Pre-exposure effects on crack initiation of L-oriented DS GTD-111 in static air under (a) pre-exposure (100hr, 982°C, -100MPa) and fatigue ($\Delta\epsilon=0.8\%$ and 871°C) and (b) pre-exposure (100hr, 982°C, 100MPa) and fatigue ($\Delta\epsilon=0.5\%$ and 871°C).

Damage Mechanism Maps

Damage mechanism maps (DMMs) are used to associate damage mechanisms with experimental conditions. For example, maps for a given mechanical strain range are shown in Fig. 9 for $\Delta\epsilon = 1.0\%$. These maps show how various types of damage arise within a given temperature versus hold time graph. The type(s) of damage responsible for crack initiation at each point is categorized based on microscopic analysis. Since the damage mechanism leading to crack initiation depends on temperature, hold time, and hold type, the contributions of each mechanism varies slightly from point to point. For experiments with tensile hold periods at high temperature, the dominant mechanism causing crack initiation is enhanced slip at defects. Intense slip and deformation at carbide leads to crack nucleation at grain boundaries, dendrite cores, and interdendritic regions. Once microcracks coalesce, they form longer cracks that connect adjacent inclusions. For longer hold times these cracks tend to follow interdendritic paths and GBs similar to specimens subjected to pure creep conditions [1].

When the hold type changes from tensile to compressive, the damage mechanism also changes. Oxide spiking was observed in several cases; however, if the temperature is too high or too low, then alternate damage mechanisms dominate. For example, if the temperature is too low, then oxidation will not occur and the mechanism will be related to fatigue; alternately, if the test temperature is too high (e.g. above 1038°C), then the majority of the mechanical strain will be dominated by plastic strain leading to creep and fatigue dominant crack initiation. A fatigue dominant crack initiation regime separates the regions corresponding to creep-fatigue and fatigue-oxidation damage. The region widens at lower temperatures at which creep is irrelevant.

Long term creep-fatigue testing with tensile dwells emphasizes traditional creep related damage mechanisms not evident in HC testing. As the time length of the dwell period was increased for HT cases, the creep-fatigue test resembled the strain-controlled, stress relaxation test. Similar to load-controlled, creep deformation tests, these experiments isolate the time-dependent inelastic behavior of the material. As such, applying longer dwell times helps to emphasize creep-related damage mechanisms. Several creep-fatigue experiments were conducted with hold times of 10 min. The main difference between the samples subjected to HC and HT conditions with longer dwell periods is that the surface cracks from the HT-tested sample are wavier than those of the HC-tested case. This is an indication of the influence on subsurface features on crack initiation and early propagation found in L-oriented DS GTD-111 when cycled under nominally tensile conditions. In compression, crack incubation and early crack propagation are oxidation-assisted.

The mapped forms of damage are not unique to the combination of strain range, strain ratio, and strain rate applied. Either the balance of several damage mechanisms or the dominance of one mechanism can be attained under other conditions. Altering the strain range effects the contributions of the mechanisms, but because only one strain level is mapped, the strain range effect is not represented in Fig. 9. For example, increasing $\Delta\epsilon$ has the effect of limiting the oxide spiking mechanism for HC cases. Alternately, surface cracking is more dominant when cycling at 0.8% strain, as shown in Fig. 5a.

Under tensile creep-fatigue conditions the surface crack will either propagate to the interdendritic regions or cause a stress concentration that will hasten the formation of subsurface voids and microcracks. Both grain boundary cracks occurred near the surface and exhibit oxide layers that are very uniform. The reduction in life caused by introducing a tensile hold time at high temperature is more drastic for the T-oriented case. For example, at temperature of 1038°C and strain range of 1.0% under HT, L and T samples exhibited a difference in lives by a factor 8.6. The difference was only 3.9 for CC under the same $\Delta\epsilon$ - T combination. The larger quantity of grain boundaries present in the T-oriented case implies increased potential sites for crack initiation.

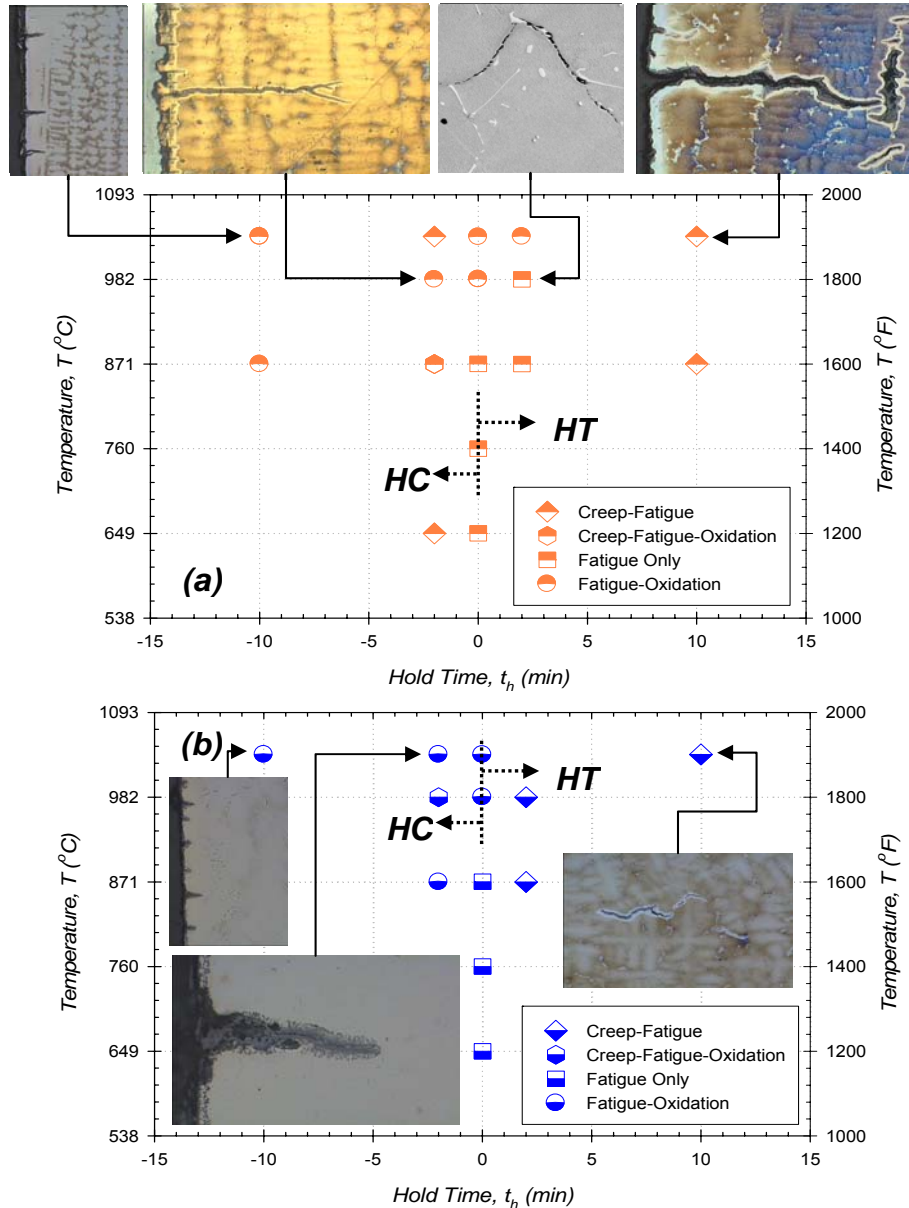


Figure 9: Damage mechanism map of crack initiation of isothermal, creep-fatigue cycled (a) L- and (b) T-oriented DS GTD-111. For each case, $\Delta\varepsilon=1.0\%$ and $\dot{\varepsilon} \geq 0.5\%/s$.

Conclusions

Using a variety of experimental configurations, interactions of fatigue, creep, and oxidation have been investigated for DS GTD-111. Conditions that lead to three distinct forms of damage were observed: oxide spiking, microcrack nucleation at carbides within dendritic cores, and microcrack nucleation at carbides within interdendritic regions. It was determined that the dominant form of damage facilitating crack initiation depends not only the test parameters involved, but also the atmosphere and the condition of the material upon fatigue cycling. Under continuous cycling conditions, cracking at carbides in dendritic regions was the dominant damage mechanism. If the surface of the material contains an oxide layer prior to fatigue cycling, then the oxide spiking mechanism contributes to crack initiation. Oxide spiking, the key mechanism leading to crack initiation under compressive creep-fatigue conditions in air, was eliminated by removing oxygen from the environment. Cracks were observed to form at interdendritic regions by means of tensile creep-fatigue cycling. Pre-exposing the material to tensile-creep conditions manifests this damage form under subsequent continuous cycling conditions.

Acknowledgements

Ali P. Gordon is grateful for the support of an ONR fellowship in conducting this research.

References

1. Ibanez, A. R., "Modeling Creep Behavior in a Directionally Solidified Nickel Base Superalloy." PhD Thesis, Georgia Institute of Technology, Atlanta, GA, (2003).
2. Sehitoglu, H. and Boismier, D. A., "Thermo-Mechanical Fatigue of Mar-M247: Part 1-Experiments." *Journal of Engineering Materials and Technology*, **112(1)**, 68-79 (1990).
3. Okazaki, M., Tabata, T. and Nohmi, S., "Intrinsic Stage I Crack Growth of Directionally Solidified Ni-Base Superalloys During Low-Cycle Fatigue at Elevated Temperature." *Metallurgical Transactions A*, **21**, 2201-2208 (1990).
4. MacLachlan, D. W. and Knowles, D. M., "Creep-Behavior Modeling of the Single-Crystal Superalloy CMSX-4." *Metallurgical and Materials Transactions A*, **31**, 1401-1411 (2000).
5. Das, D. K., Singh, V. and Joshi, S. V., "High Temperature Oxidation Behaviour of Directionally Solidified Nickel Base Superalloy CM-247LC." *Materials Science and Technology*, **19(6)**, 695-708 (2003).
6. Valerio, P., Gao, M. and Wei, R. P., "Environmental Enhancement of Creep Crack Growth in Inconel 718 by Oxygen and Water Vapor." *Scripta Metallurgica et Materialia*, **30(10)**, 1269-1274 (1994).
7. Srinivas, S., Pandey, M. C. and Taplin, D. M. R., "Air-Environment-Creep Interaction in a Nickel Base Superalloy." *Engineering Failure Analysis*, **2(3)**, 191-196 (1995).
8. Evans, H. E. and Taylor, M. P., "Creep Relaxation and the Spallation of Oxide Layers." *Surface and Coatings Technology*, **94-95**, 27-33 (1997).
9. Antolovich, S. D., Liu, S. and Baur, R., "Low Cycle Fatigue Behavior of Rene 80 at Elevated Temperature." *Metallurgical and Materials Transactions A*, **12**, 473-481 (1981).
10. Reuchet, J. and Rémy, L., "Fatigue Oxidation Interaction in a Superalloy - Application to Life Prediction in High Temperature Low Cycle Fatigue." *Metallurgical Transactions A*, **14(1)**, 141-149 (1983).
11. Wright, P. K. and Anderson, A. F., "Influence of Orientation on the Fatigue of Directionally Solidified Superalloys." *4th International Symposium on Superalloys*. J. K. Tien et al., Eds., Seven Springs, PA, American Society for Materials, pp. 689-698 (1980).
12. Shenoy, M. M., Gordon, A. P., Neu, R. W., and McDowell, D. L. "Thermomechanical Fatigue Behavior of a Directionally Solidified Ni-Base Superalloy." *Journal of Engineering Materials and Technology*, **127**, 325-336 (2005).